
# *Petrography, ascent rate, and cooling history of Cabezon Peak magma, New Mexico*

Fraser Goff and James A. Stimac, [eds.]
2024, pp. 291-298. https://doi.org/10.56577/FFC-74.291

*in:*

*Geology of the Nacimiento Mountains and Rio Puerco Valley*, Karlstrom, Karl E.;Koning, Daniel J.;Lucas, Spencer G.;Iverson, Nels A.;Crumpler, Larry S.;Aubele, Jayne C.;Blake, Johanna M.;Goff, Fraser;Kelley, Shari A., New Mexico Geological Society 74 th Annual Fall Field Conference Guidebook, 334 p.

*This page is intentionally left blank to maintain order of facing pages.*

New Mexico Geological Society Guidebook, 74th Fall Field Conference, 2024, p. 291–298, https://doi.org/10.56577/FFC-74.291


# PETROGRAPHY, ASCENT RATE, AND COOLING HISTORY OF CABEZON PEAK MAGMA, NEW MEXICO

FRASER GOFF[1] AND JAMES A. STIMAC[2]

[1]Department of Earth and Environmental Science, New Mexico Institute of Mining and Technology, 801 Leroy Place, Socorro, NM 87801; candf@swcp.com
[2]Stimac Geothermal Consulting, 342 Whiteoaks Drive NE, Albuquerque, NM 87122

**Abstract**—Cabezon Peak is a 180-m-tall trachybasalt (alkali basalt) volcanic plug (neck) that has been exposed by erosion of an original volcanic edifice and enclosing sedimentary deposits since emplacement at 2.66±0.66 Ma. The main body consists of dark-gray, columnar-jointed intrusive rock overlain by about 40 m of black to gray, massive to scoriaceous lava. Deep erosion has obscured whether the intrusion was formed beneath a scoria cone or maar/diatreme volcano. Samples of the lava are aphyric to fine-grained holocrystalline containing very sparse phenocrysts of olivine and augite and microphenocrysts of plagioclase, olivine, augite, titanomagnetite, and trace apatite. Because Cabezon Peak lava and intrusive rocks are so phenocryst-poor, it is surmised that the original magma was emplaced at a temperature of about 1200°C, well above the liquidus temperature. The lava also contains xenocrysts (a few percent) and sparse (<0.1%) xenoliths of peridotite (lherzolite), most of which are ≤0.25 cm in diameter. However, a rare lherzolite xenolith 35 cm in diameter was found. We used reasonable parameters for densities and viscosity applied to the Stokes equation for gravitational settling in a liquid to calculate an estimated minimum ascent rate of 3.9 m/sec (14 km/hr) for Cabezon magma, which is in line with published ascent rates of 2–10 m/sec for other trachybasalt magmas. Assuming Cabezon magma originated in the mantle, the time to rise from about 50 km depth to the surface is roughly 3.6 hr. In this scenario, the lag time before initial eruption of magma at the surface and first appearance of large 35 cm xenoliths would be about 35 hr. However, small, disaggregated xenolith fragments (≤1 cm) would appear at the onset of the eruption. Columnar jointing of the main intrusive mass formed during initial cooling of the plug. Column width is greater than in most lava deposits but is similar to plugs (vents) and endogenous domes of equivalent dimension to Cabezon.

## INTRODUCTION

The Rio Puerco necks are an outstanding example of a basaltic volcanic field where lava flows and enclosing sediments have been eroded away to expose their vents (necks or plugs) that produced flows (Crumpler, 2010; Bland, 2022). The Puerco necks are the eroded northeastward extension of Mesa Chivato (Fig. 1), part of the greater 3.7 to 1.26 Myr Mount Taylor volcanic field (Goff et al., 2019). All of the volcanism is part of the greater Jemez volcanic lineament (JL; Goff and Kelley, 2020). Seismic work by Sosa et al. (2014) shows that the JL along the Mesa Chivato-Mount Taylor region is underlain by probable upwelling mantle that produces mostly basalt eruptions. The basaltic products are primarily trachybasalt (alkali basalt), although there are a few other types (Crumpler, 1980; Goff et al., 2019, 2020). The object of this paper is to describe the petrology of the Cabezon intrusion and to calculate the ascent rate of Cabezon magma using the diameter of a large peridotite xenolith and other chemical and physical properties of the magma.


FIGURE 1. Satellite image of the various features around the Puerco necks and northeast Mesa Chivato. Cabezon Peak is located in the upper right corner of this map (from Crumpler, 2010).

## GEOLOGIC BACKGROUND

Cabezon is the largest of the Puerco necks (Fig. 2) and is dated at 2.66±0.06 Ma (Hallett et al., 1997). The neck (plug) is roughly 305 m in diameter and 180 m high from the base of the cliffs to the summit. Because the enclosing sediments were mostly soft Mancos Shale (Cretaceous), erosion of surface sediments and lava flows occurred rather quickly. The cliffs expose a variety of columnar joints and other textures, which result from complex cooling of fluid basalt (probably

FIGURE 2. Photograph of Cabezon Peak (2.66 Ma) looking northeast, as viewed from the neighboring plug of Cerro de la Guadalupe in August 2022. The stately monolith intrudes easily erodible, near-horizontal beds of Cretaceous Mancos Shale.

≤1200°C; Lesher and Spera, 2015) against former sedimentary rock walls.

Overall, the peak is composed of at least two distinctive subunits (Fig. 3). The main body consists of columnar jointed intrusive rock, but the capping section is massive to scoriaceous basaltic lava that is about 40 m thick (Brown, 1969; Hallett, 1992, fig. 6.2). Brown (1969) noted that most columns are 6–8 in. (15–20 cm) in diameter and that columns flare 30–45° outward towards their base. Hunt (1938) described columns ranging from about 24 to 96 in. or 61 to 244 cm, which is more consistent with our observations. Figure 3 shows part of the south wall that has about 60 columns. Black basalt above the contact with the interior is nearly aphyric (fast chilling) and scoriaceous (from degassing of volatiles), while much of the basalt near the interior is dark gray and slightly coarser-grained from slower cooling. Some lava surfaces are spotted with subtle white to pale gray radiating clots of small plagioclase crys-


FIGURE 3. Close-up photo shows part of the south face of Cabezon Peak consisting of lower intrusive rocks with columnar jointing and the overlying volcanic unit consisting of lava and scoria. The intrusive section in this photo consists of approximately 60 semicontinuous columns ranging from about 60 to 180 cm in width based on visual estimates.

tals ≤1 mm long—a common attribute of solidified trachybasalt (Goff et al., 2019).

## PETROCHEMISTRY AND MINERALOGY

Cabezon basalt is classified as borderline trachybasalt to basalt on an alkali-silica diagram (La Bas et al., 1986). Five samples analyzed by Hallett (1992, table 7.1) average 48.3±0.3 wt% $SiO_2$ and 5.13±0.12 wt% $Na_2O + K_2O$. Aphyric lava contains very sparse phenocrysts of olivine and augite in a glassy matrix. Coarser-grained lava that cooled more slowly within the plug contains the above phenocrysts and microphenocrysts visible with a hand lens of olivine, augite, plagioclase, iron oxides, and minor matrix glass.

The underlying intrusive rock composing the main colonnade section is quite homogeneous in texture, mineralogy, and composition (Figs. 4 and 5). It is fine-grained and holocrystalline, consisting mainly of plagioclase, olivine, augite, titanomagnetite, and trace apatite (Table 1). It contains very sparse vesicles and more common diktytaxitic voids, most of which are filled by secondary minerals (Fig. 5A). The diktytaxitic texture indicates that some exsolution of the primary dissolved volatiles occurred during the later stages of solidification (Goff, 1996). Cavity-filling secondary minerals include calcite, zeolites, and clays. Iddingsite, a common alteration product of olivine, forms rims on some crystals.

TABLE 1. Major mineral abundances in the main Cabezon Peak intrusive based on the average of three thin sections. Calcite, chalcedony/quartz, smectite, smectite-chlorite, zeolites, and iddingsite are present as secondary phases, mostly in vesicles and diktytaxitic voids. Pl = plagioclase; Ol = olivine; Cpx = clinopyroxene; Mt = titanomagnetite; Chr = chromite as inclusion in Ol; and Ap = apatite.

| Pl | Ol | Cpx | Mt | Chr (i) | Ap | Filled voids | Total |
|---|---|---|---|---|---|---|---|
| 50 | 25 | 18 | 6 | <0.1 | 0.2 | 0.7 | 100 |

Very few phenocrysts are present in the main intrusive body, although Brown (1969) noted olivine up to 6 mm, which he interpreted as xenocrysts. In our samples, we observed olivines up to 2 mm that were anhedral and fractured, consistent with Brown's interpretation (see Fig. 4B). We also identified clinopyroxene with cores showing fine remnant exsolution lamellae (probably orthopyroxene), indicating a xenolithic origin. Our observations indicate tiny xenocrysts are common (up to 5%). On the other hand, mantle xenoliths (lherzolite, consisting of olivine, orthopyroxene, chrome diopside, and chrome spinel) are sparse (<0.1%). Thus, finding mantle peridotite xenoliths takes some looking because most, but not all, are quite small.

Eruption style, xenolith composition, and xenolith concentration at Cabezon is quite different from those described at some other plugs in the Puerco necks. For example, Cerrito Negro consists primarily of pyroclastic breccia containing abundant lherzolite and pyroxenite xenoliths as well as upper crustal debris (Porreca et al., 2006). In fact, Cerrito Negro contains rare fragments of garnet pyroxenite. Some garnet pyroxenites contain calcite indicating mantle carbon sources; equilibration temperatures of such pyroxenites are as high as 1145°C, and the indicated source pressure is 16–18 kbar (≤67

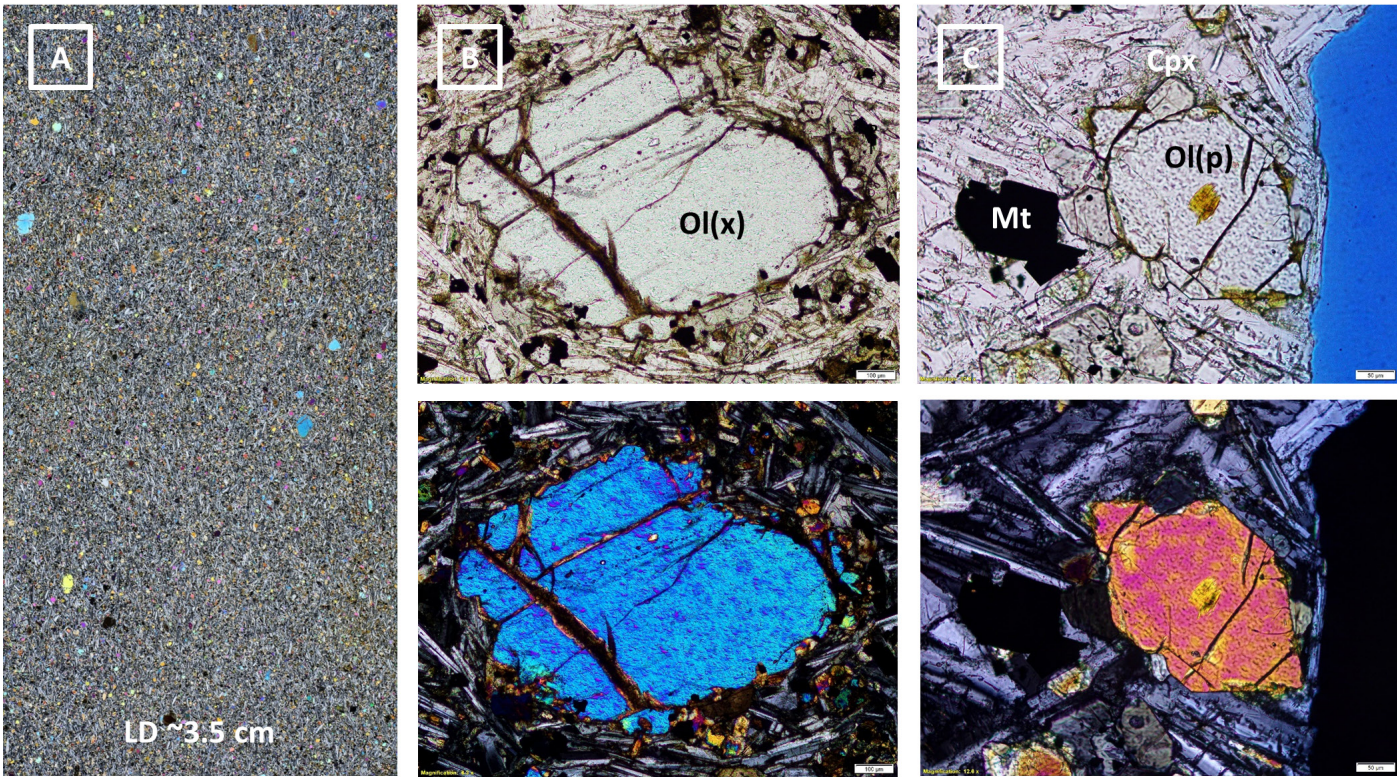


FIGURE 4. Petrography of the Cabezon intrusion in plane light (PL) and cross-polarized light (XPL). (A) Fine-grained intrusive with anhedral olivine xenocrysts (larger grains); LD = 35 mm. (B) olivine xenocryst; (C) olivine phenocryst with clinopyroxene overgrowths, titanomagnetite, and plagioclase. See Table 1 for mineral abbreviations.

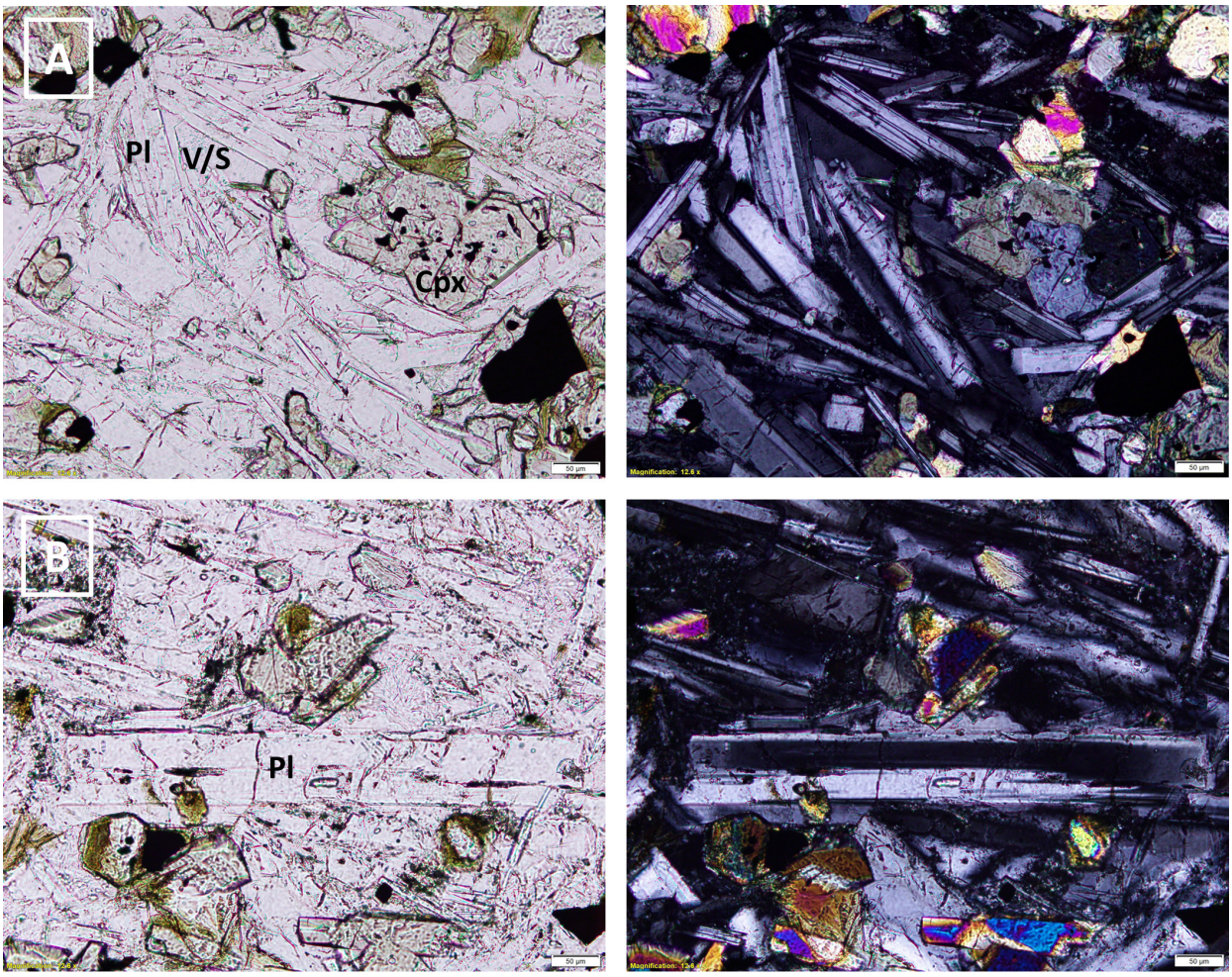


FIGURE 5. Photomicrographs of thin sections. (A) Matrix minerals with filled diktytaxitic void (V). (B) elongate plagioclase phenocryst (LM about 1 mm).

km depth, assuming a geostatic pressure gradient of 270 bars/km). The varied compositions of xenolith suites throughout the Puerco necks, Mesa Chivato, and Mount Taylor regions suggest source regions between 50 and 80 km deep (Porreca et al., 2006; Goff et al., 2013b).

## ASCENT RATE DETERMINATION

While climbing around the upper talus apron of Cabezon, the first author found an extremely large peridotite xenolith about 35 cm in diameter (Fig. 6). Large xenoliths can be used to determine the ascent rate of basaltic magmas using the Stokes Law equation for gravitational settling and knowledge of the physical properties of peridotite and liquid basalt (e.g., Spera, 1984; Rutherford and Gardner, 2000). Keep in mind that the ascent rate must be greater than the settling rate (terminal velocity, $V_t$); otherwise the large xenolith would not reach the surface. The basic equation is

$$V_t = \frac{g\,(d^2)\,(\rho_x - \rho_m)}{18\mu}$$

where g = acceleration of gravity, d = xenolith diameter, $\rho_x$ = xenolith density, $\rho_m$ = magma density, and $\mu$ = magma viscosity. In this case, we assume the xenolith is spherical, the density of peridotite (mostly olivine) is 3.3 g/cm$^3$, and the density of trachybasalt is 2.7 g/cm$^3$.

Major variables to consider in the Stokes equation are xenolith size and shape and the viscosity of basaltic magma as a function of temperature and water content. The 35-cm-diameter peridotite used in the following calculations is more or less spherical. Xenoliths larger than 35 cm (although we found none) would increase our resulting calculation of $V_t$, indicating a faster ascent rate. The quantity of water and other volatiles lowers the viscosity of all magmas (Jaupart, 2000), which also would increase ascent rate.

Magma viscosity as a function of temperature can be calculated from a chemical analysis of the lava using the empirical methods of Shaw (1972; see also Goff, 1996) or calculations from experimental melt data (Hui and Zhang, 2007; Giordano et al., 2008). Viscosity as a function of temperature is most easily visualized by plotting ln $\mu$ versus temperature (Fig. 7; Goff and Goff, 2013). In the example of Figure 7, an average of two samples of trachybasalt containing 48.3±0.4 wt% $SiO_2$ and 5.67±0.12 wt% total alkalis (Goff and Goff, 2013, and unpublished data) was used to evaluate settling of peridotite xenoliths in a trachybasalt lava flow on the west flank of Mount Taylor. The overall composition of this lava and

FIGURE 6. Large altered mantle xenolith roughly 35 cm in diameter within Cabezon trachybasalt. Most of the xenolith has weathered away, leaving an interior rind of oxidized peridotite. The specimen was broken with a hammer to verify the interior was peridotite. Note the crack line and freshly exposed light-gray trachybasalt (the hammer handle is 46 cm long).

Cabazon trachybasalt are very similar in terms of viscosity calculations; slighter higher alkali contents of the Mount Taylor lava (which lower viscosity) are offset by higher contents of ferromagnesian elements in Cabezon magma (which raise viscosity). Thus, considering all the inherent errors, Figure 7 provides a suitable representation of viscosity versus temperature for Cabezon magma.

Because Cabezon magma was aphyric, the temperature of the erupting magma was probably well above the liquidus temperature, or about 1200°C (Lesher and Spera, 2015). This corresponds to a calculated viscosity of 14.7 Pa-s (1.47 x $10^2$ poise; Shaw, 1972), or if using Figure 7, a ln Pa-s value of 2.68. The empirical methods of Shaw (1972) yield equivalent results to the experimental methods (Hui and Zhang, 2007; Giordano et al., 2008, fig. 5) because at higher temperatures (≥1100°C) and lower viscosities (ln Pa-s ≤4), basaltic liquids behave more like Newtonian fluids (due to Arrhenian temperature dependence) inherent in the Shaw model. Thus, we were content to use the Shaw model for our viscosity calculations.

If the starting composition of trachybasalt includes 0.5 wt% water (e.g., Johnson et al, 1994), a somewhat lower and more realistic viscosity of 10.3 Pa-s at 1200°C (ln Pa-s = 2.33, Fig. 7) is obtained. Addition of a reasonable amount of water lowers calculated viscosity by about 30%. For comparison, a value of 10 Pa-s is the approximate viscosity of fresh honey at room temperature, although this value depends on water content and the type of pollen bees are using at any given time (e.g., Yannoitis et al., 2006; Nayik et al., 2016).

Using the equation above and values for viscosity, density, and object diameter discussed in the text, the resulting gravitational settling rate is 389 cm/s (3.9 m/s) or 14 km/hr. Thus, the magmatic ascent rate must be ≥3.9 m/sec. If we consider possible uncertainties in parameter values, we estimate an error in ascent rate of ≤20%. Published ascent rates for trachybasalt (alkali basalt) magmas range from 2 to 10 m/sec (Rutherford and Gardner, 2000, p. 214; Russell and Jones, 2023). Mantle basalts in this region originate at ≥50 km depth (Perkins et al., 2006; Porreca et al., 2006), so in our example for a 35-cm-diameter xenolith, the minimum time to rise to the surface from mantle depths (50 km) is roughly 3.6 hr. If we assume a depth of 80 km (Porreca et al., 2006), the time would be roughly 5.8 hr. Clearly, most basaltic magmas ascend rapidly through cracks, fissures, or faults from great depths.

Another factor to consider in ascent rate is the fluid mechanical behavior of magma in the conduit or feeder dike. Pure Stokes Law behavior is favored by laminar flow of magma, whereas turbulent flow in a conduit or feeder dike retards ascent rate. A dimensionless parameter called the Reynolds number (Re; e.g., Jaupart, 2000; Russell and Jones, 2023) can evaluate laminar versus turbulent flow:

$$Re = \frac{\rho W R}{\mu}$$

where ρ = magma density, W = flow velocity, R = conduit width, and μ = bulk viscosity in conduit. However, this equation cannot predict the percentage retardation of ascent rate. The conduits for the alkali basalts in the Puerco necks, Mesa Chivato, and Mount Taylor region are dikes (e.g., Crumpler, 2010; Goff et al., 2013a), and typical dike widths exposed at the surface are around 1.5–3 m wide. Using a conduit width of 3 m, a "wet" viscosity of 10.3 Pa-s, and an ascent rate of 4 m/s, the resulting Re value is 3145. Thinner dikes have smaller values of Re, assuming other variables are constant. Above a threshold value of 1, magma in a dike would display some turbulent behavior (Jaupart, 2000), but Russell and Jones (2023) pointed out that Re >1 "does not negate the high settling rates of xenoliths in low-viscosity magmas. It simply means that xenoliths are settling at a rate that is not necessarily the ex-

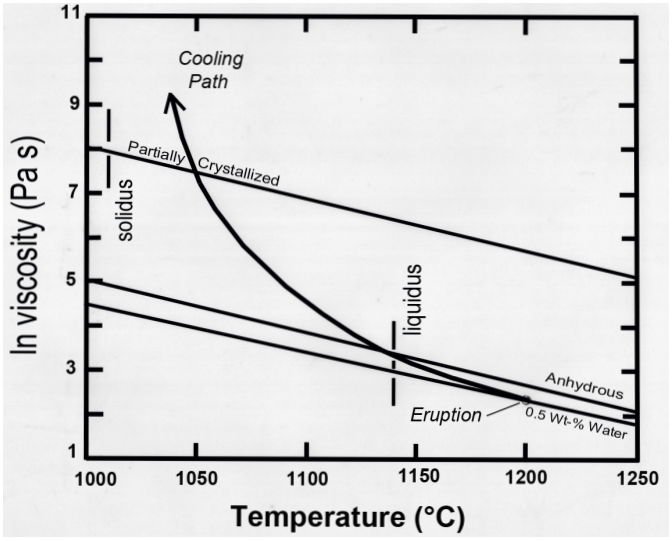


FIGURE 7. Plot of ln viscosity versus temperature for "wet," anhydrous, and partially crystallized trachybasalt following methods of Shaw (1972, tables 1 and 2, equation 3). The partially crystallized case assumes 60% crystals and 10% bubbles (Goff, 1977, p. 125). The "cooling path" shows the change in viscosity of lava from initial eruption (assumed 1200°C) to static crystallization (≤1100°C).

act velocity predicted by Stoke's Law" (p. 179). Interestingly, many of the variables of the two equations used herein are intertwined. Higher viscosity and thinner dike width favor lower values of Re.

Russell and Jones (2023, fig. 5) note a lag time exists between the first eruption of magma at the surface and the first appearance of xenoliths in the vent. Using their curves and our parameters (50 km depth, 3.9 m/s ascent rate), a 35-cm-diameter xenolith would arrive to the surface roughly 35 hr after the eruption begins. If the source region is 80 km deep, the lag time for first appearance of large xenoliths would be >60 hr. However, the arrival of tiny xenocryst fragments (≤1 cm in diameter) would occur simultaneously with the initial eruption.

## COOLING, CRYSTALLIZATION, AND COLUMNAR JOINTING

Post-emplacement cooling of the main intrusive appears to have been relatively steady and uniform based on field observations and limited sampling. Although the rock is holocrystalline, all minerals in the intrusion that are not derived from xenoliths are <1 mm in long dimension (LD). Most grains are <0.2 mm in LD but a minority reach lengths of 0.4 to 1 mm (Figs. 4 and 5). Olivines <1 mm are euhedral to subhedral and commonly partially rimmed by clinopyroxene (Fig. 4C). Plagioclase crystals are the most elongated major phase crystals, reaching 1 mm; width to length ratios are 1:10 to 3:10 (Fig. 5B). Excluding xenolithic debris, the small crystal size indicates rapid ascent of a nearly aphyric magma from its source region. However, the holocrystalline matrix of the intrusive indicates slower cooling than lava flows of the same composition.

Columnar jointing is common when a mass of fluidal magma accumulates without immediate quenching, fragmentation, or brecciation. Thus, many lava flow and dome interiors, solidified lava lakes, and near-surface intrusions display this fascinating style of jointing. Columnar jointing is formed in magmatic rocks as the result of thermal contraction during cooling (DeGraff and Aydin, 1987; Hetényi et al., 2012; Phillips et al., 2013, and references therein). A reduction in the volume of magma occurs as it cools and crystallizes, resulting in tensional forces and eventual jointing into pseudo-hexagonal columns. Normally distributed columns with four to eight sides are observed. But Akiba et al. (2021) showed that columns have a tendency toward mean pentagonal shapes with smaller diameters at rapid cooling rates and mean hexagonal shapes with larger diameters at slower cooling rates.

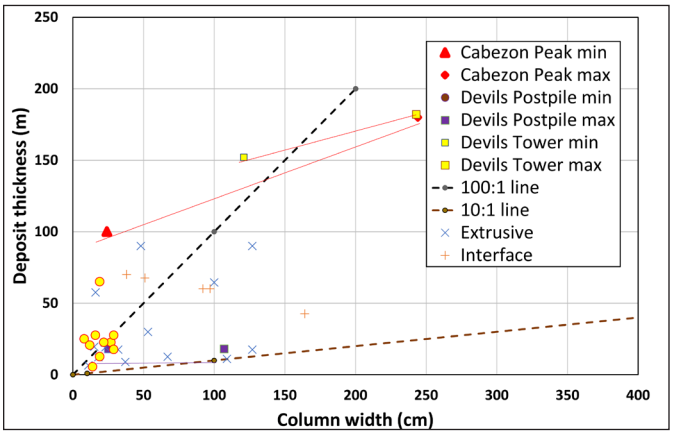


FIGURE 8. Plot of column-face width (cm) versus column height or columnar-jointed deposit height (m) modified from Hetényi et al. (2012). Data are from Hunt (1938) for Cabezon Peak, Robinson (1956) for Devils Tower, the U.S. National Park Service website for Devils Postpile, and Hetényi et al. (2012) and Phillips et al. (2013) for occurrences in Europe and Iceland. Interface refers to lava lake deposits. Column widths scale with deposit thickness, among other factors.

Columns grow perpendicular to the main cooling surfaces. Plugs such as Cabezon Peak cool mainly from the top down, resulting in long vertical columns that may flare out at depth. This has been attributed to cooling from the sides as well as "top-down" cooling at deeper levels. Devils Tower in Wyoming is another prime example of such a plug (Robinson, 1956; Halvorson, 1980; Závada et al., 2015).

Columns grow incrementally as cooling proceeds. Each increment of stress relief extends the bounding joints downward, producing a series of "chisel marks" on the column faces. Studies cited above agree that the length of a polygon-bounding fracture segment is a function of the cooling rate. Slower cooling creates wider (stouter) columns; faster cooling creates narrower (slenderer) columns. Moreover, since the width of the chisel marks depends on the spatial (vertical for lava or sill) gradient of temperature, the column width and striae, or chisel mark width, are interrelated (Phillips et al., 2013; Akiba et al., 2021). For a given magma composition, glass content is usually proportional to the cooling rate. Slower cooling results in higher crystallinity, while faster cooling results in increased glass content of the rock. Magmas solidifying as glassier rocks are expected to have slenderer columns than more crystalline rocks. Down-flowing groundwater has been implicated as the main driver of cooling, fostering convective flow and enhanced heat dissipation (Akiba et al., 2021).

We have not made detailed measurements of column widths at Cabezon Peak, but our visual estimates suggest most columns are from 60 to 180 cm in width. Previous workers have indicated a range of column widths from about 61 to 244 cm (Hunt, 1938) and 15 to 20 cm (Brown, 1969). All these estimates are within the range observed from other occurrences worldwide (Hetényi et al., 2012; Phillips et al., 2013; Akiba et al., 2021). A plot comparing Cabezon Peak column face width and column height to other documented occurrences is shown in Figure 8. Judging from this comparison, large plugs such as Cabezon Peak and Devils Tower typically have relatively slower cooling rates than most lavas and lava lakes, resulting in columns ranging to greater width. One literature occurrence with greater column width is from an 80- to 100-m-thick lava flow and dome complex with a more silicic composition than Cabezon Peak (Hetényi et al., 2012); silicic magma compositions tend to result in larger column width.

The contact between fragmental extrusive material and columnar jointed intrusive material near the summit of Cabezon Peak provides the primary evidence that it represents a plug emplaced in a near circular conduit. A variation on this theme

of plug emplacement has been proposed for Devils Tower, Wyoming by Závada et al. (2015). In their view, emplacement of the intrusive body as a coulee or lava dome within a maar-diatreme volcano is more consistent with the outward flaring of columnar joints toward the base of exposure. This scenario has been observed in other locations where hydromagmatic deposits intruded by lava plugs can be studied (Latutrie and Ross, 2020; Sawada et al., 2023). More research would be required to assess this question in the case of Cabezon Peak, but at least one nearby basaltic maar-diatreme dated at 3.07±0.09 Ma has been identified south of Cabezon in a canyon on the eastern side of the Mount Taylor stratovolcano (Goff et al., 2019; Frey et al., 2021, p. 80). Maar volcanoes and their distinctive pyroclastic beds are common both on nearby Mesa Chivato (Crumpler, 1980) and around Mount Taylor (Goff et al., 2019). Thus, a maar-diatreme mode of emplacement is not entirely out of the question.

## CONCLUSIONS

Cabezon Peak is a spectacular example of a completely exposed basaltic vent (plug and transition to subaerial lava and scoria deposits) with interesting intrusive structure, columnar joint patterns, chemical composition, petrology, and sparse lherzolite xenoliths. Thus, it is a natural laboratory that allows volcanologists and petrologists to calculate magmatic properties of basaltic magmas. Using the Stokes Law equation for gravitational settling of objects in a liquid, we calculated the ascent rate of Cabezon magma to be 3.9 m/s ± 20% (14 km/hr)—within the range of 2–10 m/s for other trachybasalt magmas. The lag time between onset of eruption at the surface and first appearance of large (≤35 cm) xenoliths is ≤35 hr. If we assume Cabezon magma originated from mantle depths of 50 km, the time required to rise to the surface was about 3.6 hr. If sourced at 80 km, the ascent time would be 5.8 hr. Columnar joint parameters noted at Cabezon are similar to those at other large volcanic plugs such as Devils Tower, Wyoming. Our results and the results of those who worked here before us are merely a starting point, as much more research can and should be done on this unique feature of the New Mexico landscape.

## ACKNOWLEDGMENTS

Cathy J. Goff (Consultant, Los Alamos, New Mexico) provided an initial review of the draft manuscript. Final peer reviews were conducted by Karl Karlstrom (University of New Mexico) and Pierre-Simon Ross (INRC, Canada). Larry Crumpler (New Mexico Museum of Natural History and Science) handled the editorial responsibilities. The authors paid for all field and laboratory research and manuscript preparation.

## REFERENCES

Akiba, Y., Takashima, A., Inoue, A., Ishidaira, H., and Shima, H., 2021, Geometric attributes of polygonal crack patterns in columnar joints: Earth and Space Science, 8, e2020EA001457, https://doi.org/10.1029/2020EA001457

Bland, D., 2022, Cabezon Peak and the Rio Puerco Necks: New Mexico Bureau of Geology and Mineral Resources Geologic Tour of New Mexico, Landmarks and Other Features, https://geoinfo.nmt.edu/tour/landmarks/cabezon/home.html

Brown, W.T., Jr., 1969, Igneous geology of the Rio Puerco Necks, Sandoval and Valencia Counties, New Mexico [M.S. thesis]: Albuquerque, University of New Mexico, 89 p.

Crumpler, L.S., 1980, Alkali basalt through trachyte suite and volcanism, Mesa Chivato, Mount Taylor volcanic field, New Mexico, Part II: Geological Society of America Bulletin, v. 91, p. 1293–1313, https://doi.org/10.1130/GSAB-P2-91-1293

Crumpler, L.S., 2010, Cabezon Peak and the Rio Puerco volcanic necks, *in* Price, G.L., ed., The Geology of Northern New Mexico's Parks, Monuments and Public Lands: Socorro, New Mexico Bureau of Geology and Mineral Resources, p. 61–67.

DeGraff, J.M., and Aydin, A., 1987, Surface-morphology of columnar joints and its significance to mechanics and direction of joint growth: Geological Society of America Bulletin, v. 99, p. 605–617, https://doi.org/10.1130/0016-7606(1987)99<605:SMOCJA>2.0.CO;2

Frey, B.A., Goff, F., Kelley, S.A., and Kelley, R.E., 2021, Day 3 road log: Cubero to Seboyeta to L-Bar Ranch, *in* Frey, B.A., Kelley, S.A., Zeigler, K.E., McLemore, V.T., Goff, F., and Ulmer-Scholle, D.S., eds., Geology of Mount Taylor: New Mexico Geological Society Guidebook 21, p. 69–84, 94. https://doi.org/10.56577/FFC-71.69

Giordano, D., Russell, J.K., and Dingwell, D.B., 2008, Viscosity of magmatic liquids: A model: Earth and Planetary Science Letters, v. 271, p. 123–134, https://doi.org/10.1016/j.epsl.2008.03.038

Goff, F., 1977, Vesicle cylinders in vapor-differentiated basalt flows [Ph.D. thesis]: Santa Cruz, University of California, 181 p.

Goff, F., 1996, Vesicle cylinders in vapor-differentiated basalt flows: Journal of Volcanology and Geothermal Research, v. 71, p. 167–185, https://doi.org/10.1016/0377-0273(95)00073-9

Goff, F., and Goff, C.J., 2013, The Quarry lava flow, a peridotite-bearing trachybasalt at Mount Taylor Volcano, *in* Ziegler, K.E., Timmons, J.M., Timmons, S., and Semken, S., eds., New Mexico Geology of Route 66 Region: Flagstaff to Grants: New Mexico Geological Society Guidebook 64, p. 67–69.

Goff, F., and Kelley, S.A., 2020, Facts and hypotheses regarding the Miocene-Holocene Jemez Lineament, New Mexico, Arizona and Colorado, *in* Frey, B.A., Kelley, S.A., Ziegler, K.E., McLemore, V.T., Goff, F., and Ulmer-Scholle, D.S., eds., The Geology of the Mount Taylor Area: New Mexico Geological Society Special Publication 14, p. 1–15, https://doi.org/10.56577/FFC-71.101

Goff, F., Wolff, J.A., and Fellah, K., 2013a, Mount Taylor dikes, *in* Ziegler, K.E., Timmons, J.M., Timmons, S., and Semken, S., eds., New Mexico Geology of Route 66 Region: Flagstaff to Grants: New Mexico Geological Society Guidebook 64, p. 159–165.

Goff, F., Wolff, J.A., McIntosh, W., and Kelley, S.A., 2013b, Gabbroic shallow intrusions and lava-hosted xenoliths in the Mount Taylor area, New Mexico, *in* Ziegler, K.E., Timmons, J.M., Timmons, S., and Semken, S., eds., New Mexico Geology of Route 66 Region: Flagstaff to Grants: New Mexico Geological Society Guidebook 64, p. 143–151.

Goff, F., Kelley, S.A., Goff, C.J., McCraw, D.J., Osburn, G.R., Lawrence, J.R., Drakos, P.G., and Skotnicki, S.J., 2019, Geologic map of the Mount Taylor volcano area, New Mexico: New Mexico Bureau of Geology and Mineral Resources Geologic Map 80, scale 1:36,000, 61 p., https://doi.org/10.58799/GM-80

Goff, F., McIntosh, W., Peters, L., Wolff, J.A., Kelley, S.A., Goff, C.J., and Osburn, G.R., 2020, Volcanic evolution of Mount Taylor stratovolcano, New Mexico: Facts and misconceptions, *in* Frey, B.A., Kelley, S.A., Ziegler, K.E., McLemore, V.T., Goff, F., and Ulmer-Scholle, D.S., eds., The Geology of the Mount Taylor Area: New Mexico Geological Society Special Publication 14, p. 17–28, https://doi.org/10.56577/FFC-71.117

Hallett, R.B., 1992, Volcanic geology, paleomagnetism, geochronology and geochemistry of the Rio Puerco necks, west-central New Mexico [Ph.D. thesis]: Socorro, New Mexico Institute of Mining and Technology, 340 p.

Hallett, R.B., Kyle, P.R., and McIntosh, W.C., 1997, Paleomagnetic and $Ar^{40}/Ar^{39}$ age constraints on the chronologic evolution of the Rio Puerco volcanic necks and Mesa Prieta, west-central New Mexico: Geological Society of America Bulletin, v. 109, p. 95–106, https://doi.org/10.1130/0016-7606(1997)109<0095:PAAAAC>2.3.CO;2

Halvorson, D.L., 1980, Geology and petrology of the Devils Tower, Missouri Buttes, and Barlow Canyon area, Crook County, Wyoming [Ph.D. dissertation]: Grand Forks, University of North Dakota, 181 p., https://commons.und.edu/theses/119

Hetényi, G., Taisne, B., Garel, F., Médard, É., Bosshard, S., and Mattsson, H.B., 2012, Scales of columnar jointing in igneous rocks: Field measurements and controlling factors: Bulletin of Volcanology, v. 74, p. 457–482, https://doi.org/10.1007/s00445-011-0534-4

Hui, H., and Zhang, Y., 2007, Toward a general viscosity equation for natural anhydrous and hydrous silicate melts: Geochimica et Cosmochimca Acta, v. 71, p. 403–416, https://doi.org/10.1016/j.gca.2006.09.003

Hunt, C.B., 1938, Igneous geology and structure of the Mount Taylor volcanic field, New Mexico: U.S. Geological Survey Professional Paper 189-B, 80 p., https://doi.org/10.3133/pp189B

Jaupart, C., 2000, Magma ascent at shallow levels, *in* Sigurdsson, H., Houghton, B., Rymer, H., Stix, J., and McNutt, S., eds., Encyclopedia of Volcanoes: San Diego, Academic Press, p. 237–245.

Johnson, M.C., Anderson, A.T., and Rutherford, M.J., 1994, Chapter 8: Pre-eruptive volatile contents of magmas, *in* Carroll, M.R., and Holloway, J.R., eds., Volatiles in Magmas: Reviews in Mineralogy, Vol. 30: Fredericksburg, Virginia, Mineralogical Society of America, p. 281–330, https://doi.org/10.1515/9781501509674-014

La Bas, M.J., Le Maitre, R.W., Streckeisen, A., and Zanettin, 1986, A chemical classification of volcanic rocks based on the total alkali-silica diagram: Journal of Petrology, v. 27, p. 745–750, https://doi.org/10.1093/petrology/27.3.745

Latutrie, B., and Ross, P.-S., 2020, Phreatomagmatic versus magmatic eruptive styles in maar-diatremes: A case study at Twin Buttes, Hopi Buttes volcanic field, Navajo Nation, Arizona: Bulletin of Volcanology, v. 82, article 28, https://doi.org/10.1007/s00445-020-1365-y

Lesher, C.E., and Spera, F.J., 2015, Thermodynamics and transport properties of silicate melts and magma, *in* Sigurdsson, H., ed., The Encyclopedia of Volcanoes, volume 2: Elsevier, p. 113–141, https://doi.org/10.1016/B978-0-12-385938-9.00005-5

Nayik, G.A., Dar, B.N., and Nanda, V., 2016, Rheological behavior of high altitude Indian honey varieties as affected by temperature: Journal of the Saudi Society of Agricultural Sciences, v. 17, no. 3, p. 323–329, https://doi.org/10.1016/j.jssas.2016.07.003

Perkins, G.B., Sharp, Z.D., and Silverstone, J., 2006, Oxygen isotope evidence for subduction and rift-related mantle metasomatism beneath the Colorado Plateau–Rio Grande rift transition: Contributions to Mineralogy and Petrology, v. 151, p. 633–650, https://doi.org/10.1007/s00410-006-0075-6

Porreca, C., Silverstone, J., and Samuels, K., 2006, Pyroxene xenoliths from the Rio Puerco volcanic field, New Mexico: Melt metasomatism at the margin of the Rio Grande rift: Geosphere, v. 2, p. 333–351, https://doi.org/10.1130/GES00058.1

Phillips, J.C., Humphreys, C.S., Daniels, K.A., Brown, R.J., and Witham, F., 2013, The formation of columnar joints produced by cooling in basalt at Staffa, Scotland: Bulletin of Volcanology, v. 75, article 715, https://doi.org/10.1007/s00445-013-0715-4

Robinson, C.S., 1956, Geology of Devils Tower National Monument, Wyoming: U.S. Geological Survey Bulletin 1021–1, 13 p.

Russell, J.K., and Jones, T.J., 2023, Transport and eruption of mantle xenoliths creates a lagging problem: Communications Earth & Environment, v. 4, p. 177–186, https://doi.org/10.1038/s43247-023-00843-0

Rutherford, M.J., and Gardner, J.F., 2000, Rates of magma ascent, *in* Sigurdsson, H., Houghton, B., Rymer, H., Stix, J., and McNutt, S., eds., Encyclopedia of Volcanoes: San Diego, Academic Press, p. 207–217.

Sawada, Y., Uno, K., Sakai, T., and Hyodo, H., 2023, A solidified lava lake in an explosion crater within granitic basement, SW Japan: Bulletin of Volcanology, v. 85, article 26, https://doi.org/10.1007/s00445-023-01634-3

Shaw, H.R., 1972, Viscosities of magmatic silicate liquids: An empirical method of prediction: American Journal of Science, v. 272, p. 870–893, https://doi.org/10.2475/ajs.272.9.870

Sosa, A., Thompson, L., Velasco, A.A., Romero, R., and Herrmann, R., 2014, 3-D structure of the Rio Grande rift from 1-D constrained joint inversion of receiver functions and surface wave dispersion: Earth and Planetary Science Letters, v. 402, p. 127–137, https://doi.org/10.1016/j.epsl.2014.06.002

Spera, F.J., 1984, Carbon dioxide in petrogenesis III: Role of volatiles in the ascent of alkaline magma with special reference to xenolith-bearing mafic lavas: Contributions to Mineralogy and Petrology, v. 88, p. 217–232, https://doi.org/10.1007/BF00380167

Yannoitis, S., Skaltsi, S., and Karaburnoiti, S., 2006, Effect of moisture content on the viscosity of honey at different temperatures: Journal of Food Engineering, v. 72, p. 372–377, https://doi.org/10.1016/j.jfoodeng.2004.12.017

Závada, P., Dědeček, P., Lexa, J., and Keller, G.R., 2015, Devils Tower (Wyoming, USA): A lava coulée emplaced into a maar-diatreme volcano?: Geosphere, v. 11, p. 354–375, https://doi.org/10.1130/GES01166.1